Mutations in the neuronal β-tubulin subunit TUBB3 result in malformation of cortical development and neuronal migration defects

Karine Poirier[1,2], Yoann Saillour[1,2,†], Nadia Bahi-Buisson[1,2,3,†], Xavier H. Jaglin[1,2], Catherine Fallet-Bianco[7,8], Rima Nabbout[3,9], Laetitia Castelnau-Ptakhine[1,2], Agathe Roubertie[10], Tania Attie-Bitach[4], Isabelle Desguerre[1,2,3], David Genevieve[4], Christine Barnerias[4], Boris Keren[11], Nicolas Lebrun[1,2], Nathalie Boddaert[5], Féréchté Encha-Razavi[6] and Jamel Chelly[1,2,*]

[1]Institut Cochin, Université Paris-Descartes, CNRS (UMR 8104), Paris, France, [2]Inserm, U1016, Paris, France, [3]Service de Neurologie pédiatrique, [4]Service de pédiatrie, [5]Service de Radiologie and [6]Service d'histologie-embryologie-cytogénétique, Assistance Publique-Hôpitaux de Paris (AP-HP), hôpital Necker, Paris, France, [7]Département d'anatomie pathologique, AP-HP, hôpital saint Anne, Paris, France, [8]Inserm, U894, Paris, France, [9]Inserm, U663, Paris, France, [10]Service de pédiatrie, centre hospitalier Guy de Chauliac, Montpellier, France and [11]Génétique Chromosomique, AP-HP, hôpital Pitié-Salpétrière, Paris, France

Mutations in the *TUBB3* gene, encoding β-tubulin isotype III, were recently shown to be associated with various neurological syndromes which all have in common the ocular motility disorder, congenital fibrosis of the extraocular muscle type 3 (CFEOM3). Surprisingly and in contrast to previously described *TUBA1A* and *TUBB2B* phenotypes, no evidence of dysfunctional neuronal migration and cortical organization was reported. In our study, we report the discovery of six novel missense mutations in the *TUBB3* gene, including one fetal case and one homozygous variation, in nine patients that all share cortical disorganization, axonal abnormalities associated with pontocerebellar hypoplasia, but with no ocular motility defects, CFEOM3. These new findings demonstrate that the spectrum of *TUBB3*-related phenotype is broader than previously described and includes malformations of cortical development (MCD) associated with neuronal migration and differentiation defects, axonal guidance and tract organization impairment. Complementary functional studies revealed that the mutated βIII-tubulin causing the MCD phenotype results in a reduction of heterodimer formation, yet produce correctly formed microtubules (MTs) in mammalian cells. Further to this, we investigated the properties of the MT network in patients' fibroblasts and revealed that MCD mutations can alter the resistance of MTs to depolymerization. Interestingly, this finding contrasts with the increased MT stability observed in the case of CFEOM3-related mutations. These results led us to hypothesize that either MT dynamics or their interactions with various MT-interacting proteins could be differently affected by *TUBB3* variations, thus resulting in distinct alteration of downstream processes and therefore explaining the phenotypic diversity of the *TUBB3*-related spectrum.

*To whom correspondence should be addressed at: Institut Cochin, Université Paris-Descartes, CNRS (UMR 8104), 24 rue du faubourg st Jacques, 75014 Paris, France. Tel: +33 144412410; Email: jamel.chelly@inserm.fr
†These authors contributed equally to this work.

INTRODUCTION

Malformations of cortical development (MCD) encompass various cortical disorders that include, but are not exclusive to, the agyria–pachygyria spectrum (absent or reduced number of cortical folds) and polymicrogyria (PMG) (excessive small gyri with abnormal cortical lamination), which result in moderate to severe encephalopathies. MCD are believed to result from the alteration of several stages of cortical development from proliferation and migration of neuronal cells, to organization of their final position within cortical layers. Over the last few years, evidence demonstrating the critical role of the cytoskeleton network in proper cortical development was reported. The importance of microtubules (MTs) was further emphasized due to its association to mutations in genes encoding for α-tubulin (*TUBA1A, TUBA8*) (MIM *602529 and *605742) and β-tubulin (*TUBB2B*) (MIM *612850) subunits in lissencephaly and PMG (1–5). Moreover, neuropathological studies of *TUBA1A-* and *TUBB2B*-mutated fetus showed neuronal migration defects and features of axonal guidance disorganization. This was confirmed by investigations of the *Tuba1a*$^{S140G/+}$ mouse model and through *in utero Tubb2b* RNAi approaches. *Tuba1a*$^{S140G/+}$ mutant mice displayed hippocampus lamination defects, and *in vivo* reduction of *Tubb2b* led to aberrant radial migration (1–3). Biochemical and cellular investigations revealed α-/β-tubulin heterodimer assembly defects, which strengthened the *in vivo* data, suggesting that haploinsufficiency and MT dysfunctions underlie these migration defects.

Recently, the importance of MTs in axonal guidance was further established by Tischfield *et al*. (6) through complementary genetic and functional investigations. They have indeed shown that heterozygous *TUBB3* missense mutations (MIM *602661) are implicated in various neurological disorders encompassing either isolated congenital fibrosis of the extraocular muscle type 3 (CFEOM3) (MIM no. 600638) or in association with early- to late-onset polyneuropathy and developmental delay. Neuroimaging data of patients with *TUBB3* mutations revealed a spectrum of abnormalities that include hypoplasia of oculomotor nerves and dysgenesis of the corpus callosum and the internal capsule. In contrast to phenotypes related to *TUBA1A*, *TUBB2B* and *TUBA8* mutations (5,6), no cortical dysgenesis and gyral abnormalities were observed in *TUBB3*-related phenotypes reported by Tischfield *et al*. (6).

However, in continuation with our previous findings (1–3), we tested *TUBB3* in MCD patients with or without cerebellar defects because of its similar spatio-temporal expression to *TUBA1A* and *TUBB2B*, and showed that its implications in cortical dysgeneses are characterized by gyral abnormalities.

RESULTS

Mutations in *TUBB3* are responsible for *de novo* and inherited neurological disorders

Following a previous study focused on a patient panel with the lissencephaly–pachygyria spectrum (2) and the implication of *TUBB2B* in PMG, we expanded the screening of the *TUBB3* gene to a new cohort of 120 individuals with MCD, preferentially encompassing PMG, gyral disorganization and simplification syndromes with or without pontocerebellar defects. We identified six novel *TUBB3* missense mutations (p.G82R, p.T178M, p.E205K (recurrent), p.A302V, p.M323V and p.M388V) in 12 patients from seven independent families (3 inherited familial forms and 4 sporadic cases, Fig. 1). One mutation resides in exon 3 and five in exon 4. All of them modify highly conserved amino acids and segregate with the phenotype in each family. In the particular case of family 5 native of the northwest region of France, we identified a p.A302V *TUBB3* homozygous mutation in a young girl (F5-II) and the same heterozygous mutation in her less affected mother (F5-I). The father of the F5-II girl was not accessible for phenotypic testing and therefore his DNA was unavailable for analysis. The search for a loss of heterozygosity was performed by Illumina SNP array experiments and allowed the exclusion of the *TUBB3* deletion and revealed a high level of homozygosity for the F5-II patient, who presented the first recessive form of a *TUBB3* mutation (Supplementary Material, Fig. S1), suggesting that parents of this patient are consanguineous. For the other families, segregation analyses of *TUBB3* mutations are coherent with *de novo* or familial dominant transmission of MCD. Furthermore, all variants were not detected in 360 normal controls of Caucasian origins.

TUBB3 mutations result in cortical malformations associated with axon guidance defects

In order to better define the phenotype corresponding to *TUBB3* mutations, nine mutated patients were retrospectively re-examined (Table 1). The large majority of patients with *TUBB3* mutations were referred to paediatric neurology consultations for either delayed acquisition of developmental milestones or mental retardation at school age. On examination, all, except one (F5-1), presented axial hypotonia, and spastic diplegia or tetraplegia (three of nine, Table 1). All tested patients exhibit intermittent (three of seven) to permanent (four of seven) strabismus combined with either multidirectional (two of four) or horizontal (two of four) nystagmus. None presented ptosis or external ophthalmoplegia, and fundoscopy was normal in all cases.

The severity of mental retardation ranged from mild to severe mental retardation. All, except patient F5-I, acquired with some delay the ability to walk before the age of 3 years, and were able to use words, although speech and language development were delayed in all cases. None presented behavioural disturbance. None presented facial weakness or congenital contractures of wrist and finger or signs of polyneuropathy. Epilepsy was reported in two cases, consisting of refractory and multifocal epilepsy in one case, and occasional prolonged febrile seizures in another patient.

MRI of patients with mutations in *TUBB3* (Fig. 2) showed a common complex cortical dysgenesis that combined frontally predominant microgyria (four of nine) (Fig. 2F) or gyral disorganization and simplification (five of nine) (Fig. 2C), dysmorphic and hypertrophic basal ganglia with fusion between putamen and caudate nucleus (eight of nine), cerebellar vermian dysplasia (nine of nine), hypoplastic brainstem

Figure 1. Mutations in the *TUBB3* gene in cases of MCD. (**A**) Primary sequence of the βIII-tubulin protein showing the position of MCD-associated substitutions. (**B**) Pedigrees of families with *TUBB3* mutations reported in this study. Square, male; round, female; diamond, fetus. Black colouring, affected individual; N, normal allele; m, mutated allele.

(eight of nine) and hypoplastic corpus callosum (eight of nine) (Fig. 2 and Table 1).

Tractography studies of the corticospinal tract at the level of the posterior arm of the internal capsule reveal progressively smaller tract size and misorientation of the pyramidal fibres (Fig. 3). This analysis also revealed the presence of aberrantly oriented fibre tracts and cortical projections. These diffusion tensor imaging (DTI) studies, together with the anatomic findings of dysmorphic and hypertrophic basal ganglia with fusion between putamen and caudate nucleus, further reinforce the hypothesis that a general defect in axonal guidance is associated with *TUBB3* mutations.

Notably, the most severely affected patient (F2), with severe microcephaly and virtually no development, showed the more complex cerebral malformation, combining global gyral disorganization, complete corpus callosum agenesis and cerebellum dysplasia that also affected the hemisphere with vermian hypoplasia.

On the other hand, the less severely affected F5-I patient with mild mental retardation showed frontoparietal gyral disorganization without basal ganglia and corpus callosum abnormalities (Table 1).

Neuropathological analyses of the fetus with p.M388V *TUBB3* mutation

One of the mutations (p.M388V) was identified in a fetal case (F7) in which the pregnancy was terminated in accordance with French law at 27 weeks of gestation after a diagnosis of microcephaly and corpus callosum during an ultrasound examination. Macroscopic neuropathological analysis of the fetal brain showed micro-lissencephaly with severe brainstem

and cerebellar hypoplasia (Fig. 4A–D), olfactory bulbs agenesis, optic nerve hypoplasia and dysmorphic basal ganglia. Detailed histopathological and immunostaining analysis further disclosed abnormally voluminous germinal zones, a severely disorganized cortical plate with a festooned-like pattern (Fig. 4C, D and Supplementary Material, Fig. S2), associated with a disturbed cortical cytoarchitecture and neuronal differentiation with no clear limitation between white and grey matter (Fig. 4E, F and Supplementary Material, Fig. S2). In addition, caudate nucleus, putamen and pallidum were absent, and thalami were hypoplastic and crudely shaped (Supplementary Material, Fig. S2). Migration abnormalities were clearly suggested by abnormal cortical and hippocampal cytoarchitectony, aberrant cortical interneurons number and localization (Supplementary Material, Fig. S2E–H) and by heterotopic neurons in the white matter (Fig. 4E and F). Complementary histological examination confirmed a lack of callosal fibres and revealed the absence of corticospinal tracts. Aberrant fibre bundles were found in great quantities in the superficial cortical layer and in the periventricular regions, suggesting axonal guidance defects (Fig. 4I and J and Supplementary Material, Fig. S2I and J).

TUBB3 mutations impair the formation of α-/βIII-tubulin heterodimers

To explore the functional consequences of the mutations on TUBB3 functions, we first determined the localization of each mutation within the secondary structure of the βIII-tubulin polypeptide (7). All mutated residues (p.G82, p.T178, p.E205, p.A302 and p.M323) were localized in H–S loops (H2–B3, B5–H5, B6–H6, H9–B8 and B8–H10) and

Table 1. Summary of clinical phenotypes and MRI features associated with *TUBB3* mutations

Patient (sex/age) mutation	OFC	Motor delay	Cognitive function	Epilepsy	Ophthalmological	Cortical dysgenesis Predominant location	Type of CD	Cerebellum Cerebellar vermis	Cerebellar Hemisphere	Brainstem	Corpus callosum	Basal ganglia
F1 (M/3y) p.G82R	50th p	Axial hypotonia	Moderate MR	Absent	Strabismus	Perisylvian and frontal	Multifocal PMG / microgyria	Dysplastic	N	Hypoplastic	Posterior agenesis	Fusion caudate/ putamen hypertrophic
F2 (F/1y) p.T178M	<3rd p	Severe axial hypotonia, spastic tetraplegia	Not determined (ND)	Refractory neonatal epilepsy	Multidirectional nystagmus/ intermittent strabismus	Global gyral disorganization	Gyral disorganization	Hypoplasia	Severely dysplastic	Hypoplastic	Complete agenesis	Fusion caudate/ putamen/ hypertrophic
F3 (M/8y) p.E205K	3rd p	Mild spasticity, orofacial dyspraxia	Moderate MR	Absent	Strabismus	Perisylvian and frontal	Multifocal PMG	Dysplastic	N	Hypoplastic	Thick	Fusion caudate/ putamen/ hypertrophic
F4-I (M/10y) p.E205K	10th p	Axial hypotonia	Severe MR	Prolonged febrile seizures	Normal	Perisylvian	PMG	Dysplastic	N	Hypoplastic	Thin	Fusion caudate/ putamen
F4-II (F/14y) p.E205K	10th p	Axial hypotonia	Severe MR	Absent	Normal	Perisylvian	PMG	Dysplastic	N	Hypoplastic	Thin	Fusion caudate/ putamen
F5-II (F/1y) p.A302V	3rd p	Axial hypotonia	Not evaluable	absent	Multidirectional nystagmus/ intermittent strabismus	Frontoparietal	Gyral disorganization	Dysplastic	N	Hypoplastic	Thin	Fusion caudate/ putamen
F5-I (F/37y) p.A302V	10th p	Absent	Mild MR	Absent	Intermittent strabismus	Frontoparietal	Gyral disorganization	Dysplastic	N	N	N	N
F6-I (M/36y) p.M323V	3rd p	Axial hypotonia, spastic diplegia	Severe MR	Absent	Strabismus/horizontal nystagmus	Frontoparietal	Gyral disorganization	Dysplastic	Dysplastic	Hypoplastic	Thin	Hypertrophic/mild fusion
F6-II (M/2y) p.M323V	25th p	Axial hypotonia	Language delay	Absent	Strabismus/horizontal nystagmus	Frontoparietal	gyral disorganization	Dysplastic	N	Hypoplastic	Thin	hypertrophic/mild fusion

p., percentile; ND, not determined; y, years; MR, mental retardation; OFC, occipitofrontal head circumference; Ht, heterozygous; Hm, homozygous; N, normal; PMG, polymicrogyria.

one (p.M388V) in the H11 helix (Fig. 5A–C). Interestingly, detailed analysis showed that three residues (p.G82, p.T178 and p.M323) (Fig. 5A and B) were located in the surface area of tubulin, on the opposite side of p.R262, p.E410 and p.D417 mutations reported by Tischfield *et al*. (6) (Fig. 5D and E). According to structural data, only one mutated residue (T178) is likely to influence GTP binding as it lies in proximity to the ribose of the nucleotide. Neither of the remaining mutations seems to affect the binding pocket of βIII-tubulin.

To further investigate functional consequences of the mutations, we expressed the β-tubulin mutants in rabbit reticulocyte lysate and studied its ability to assemble into α-/β-heterodimers in the presence of bovine brain tubulin (Fig. 6). First, we found that the five mutants (p.G82R was not tested) were translated as efficiently as the wild-type control (Fig. 6A). However, analysis of the same reaction products under native conditions revealed a range of heterodimer formation that in most cases differed both quantitatively and qualitatively from the wild-type control (Fig. 6A). Though mutant p.T178M generated heterodimers with efficiency comparable to the WT control, it was remarkable to note that p.E205K, p.A302V and p.M388V mutant polypeptides yielded no discernable amount of heterodimer (Fig. 6A). The remaining mutant p.M323V did generate heterodimers, but with a diminished yield. These results reveal the impairment of tubulin heterodimerization processes in four of the five tested mutants.

Subsequently, we analysed the localization of βIII-tubulin mutants upon overexpression in different cell types. The transfection of the flag-tagged *TUBB3*-mutated constructs in COS7 and HeLa cells revealed a similar incorporation of variant βIII-tubulin proteins into MTs compared with the control (Fig. 6B and data not shown). Two mutants, p.E205K and p.M388V, produced in some cells a dotted localization pattern, suggesting a subtle impairment of its ability to incorporate into the cytoskeleton (Fig. 6B). Moreover, complementary investigations of the MT network of p.T178M and p.E205K patients' fibroblasts confirmed that no major alterations were observed in the MT network of the cells (data not shown). All biochemical and cellular results reveal that most of the mutations described in this study alter the efficiency of the tubulin heterodimerization process; this is most likely to be independent of GTP-binding mechanisms. It also suggests that the formed heterodimers are able to fully incorporate into MT networks.

TUBB3 mutations associated with MCD impair MT stability

To further assess the effect of MCD-related *TUBB3* mutations on MT dynamics, we explored MT behaviour in fibroblastic cells of two patients who, respectively, carry the p.T178M and p.E205K *TUBB3* mutations. We first showed by RT–PCR, immunocytochemistry and western blotting using the monoclonal antibody tuj1 and primary cultures of neuronal cells (used as positive control), glial cells (used as a negative control) and fibroblasts that TUBB3 is significantly expressed in fibroblasts (data not shown). In order to assess the potential consequences of these mutations on MT dynamics, we analysed the response of the cytoskeleton of fibroblasts estab-
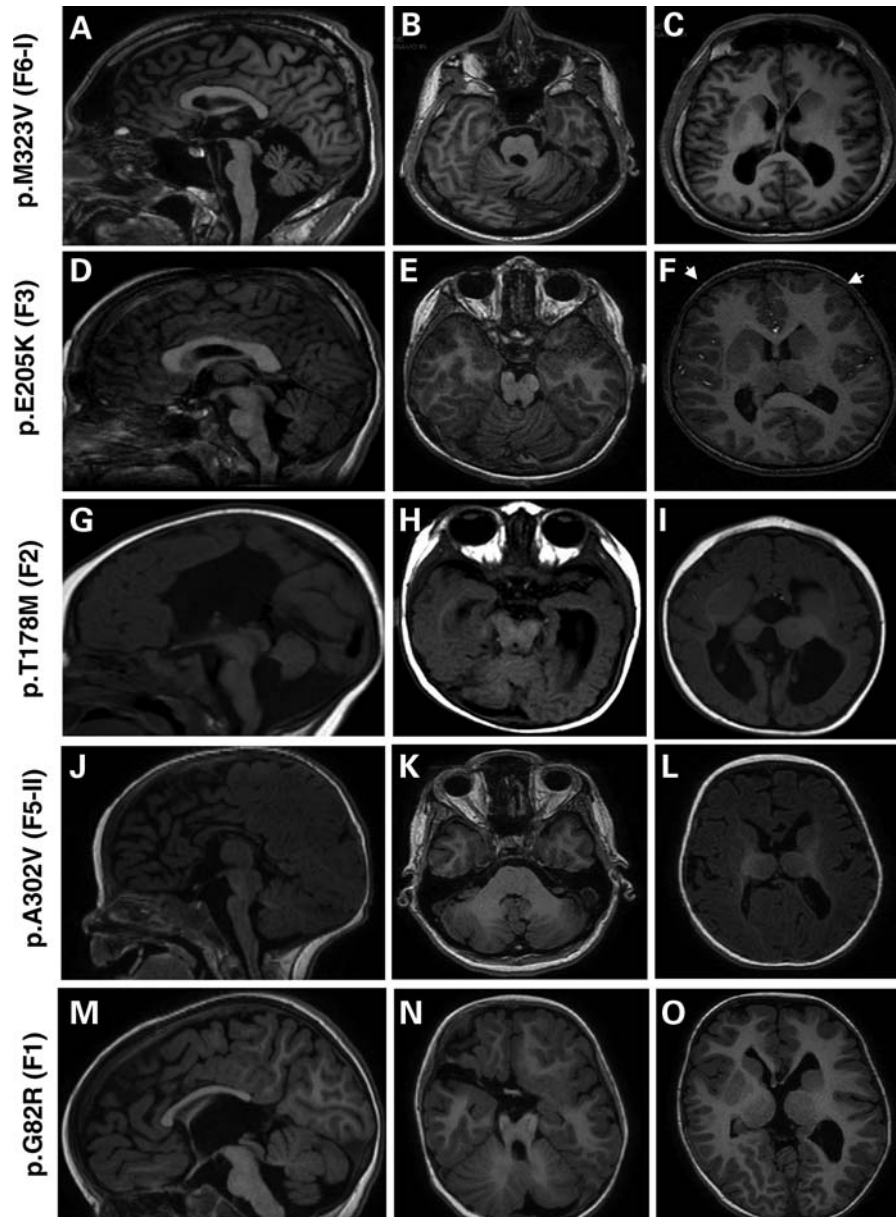
Figure 2. MRI of patients with *TUBB3* mutations (**A–O**). Midline sagittal MRI showing the spectrum of corpus callosum abnormalities in patients with *TUBB3* mutation: it appears either thick (D), thin (A and J) with an agenesis of its posterior part (M) or with a total agenesis (G). At the brainstem level, *TUBB3* mutations are associated with mild (D and M) to moderate (A, G and J) hypoplasia of the brainstem. Axial MRI at the level of cerebellar vermis shows a different degree of vermian dysplasia, severe dysplasia of the vermis and hemisphere (B and N), moderate vermian dysplasia (E) and mild vermian dysplasia (H and K) and hypoplasia of the vermis (H). Axial MRI at the level of basal ganglia shows frontally predominant microgyria (white arrows F), and gyral disorganization consisting of small gyri with parallel orientation mainly in the frontal region (C, I and O) and hypertrophic and dysmorphic basal ganglia in all cases (C, F, I and O).

lished from control and affected patients to cold-induced depolymerization treatment followed by a repolymerization step at 37°C. First, we examined by immunofluorescence staining of α-tubulin the cytoskeleton morphology and the pool of unincorporated tubulin in mutant cells at various times of cold treatment. Results corresponding to these experiments (Fig. 7) consistently showed that p.T178M and p.E205K mutations lead to decreased cytoskeleton resistance to cold treatment compared with that in control samples. We have found that complete MT depolymerization occurred after only 11 min of cold treatment for the p.T178M and p.E205K

mutants in comparison with control cells which are depolymerized after 15 min at 4°C (Fig. 7). These data suggest that mutated MTs are less stable than normal ones.

DISCUSSION

One gene, several phenotypes

In this study, we provide evidence showing that missense mutations in the *TUBB3* gene are causative of MCD associated with neuronal migration defects, white matter abnormal-
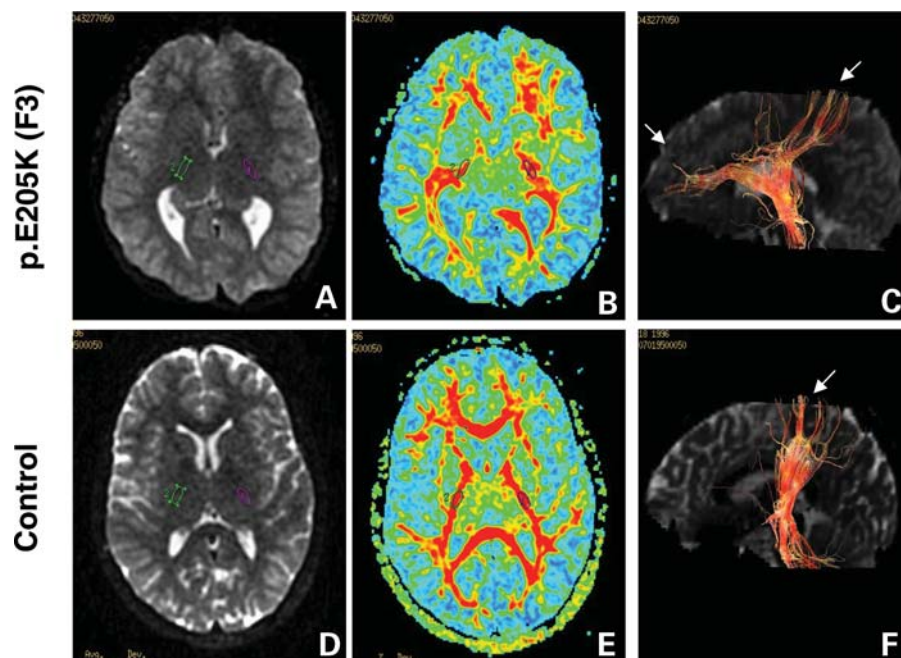
Figure 3. Diffusion tensor imaging (DTI) of corticospinal tracts in *TUBB3* mutation p.E205K (F3) and control individuals. Diffusion-weighted axial images (**A** and **E**) show dysmorphic basal ganglia with fusion between caudate and putamen, and virtually no visible anterior arm of the internal capsule, while the posterior arm appears hypertrophic in the patient with *TUBB3* mutation (A) compared with control (**D**). Green and purple circles identify regions of interest (ROI 35 mm^2) in the posterior arm of the internal capsule. DTI colour maps (**B** and E) show the dysmorphic internal capsule in patients with *TUBB3* mutation (B) compared with control subjects (**F**). For all images, colour depicts the predominant fibre direction. The vector analysis of the colour maps is assigned to red (superoinferior), green (anteroposterior) and blue (left to right). The intensities of the colour map are scaled in proportion to the fractional anisotropy (FA). Three-dimensional reconstruction in the sagittal plane of the corticospinal tract at the level of the posterior arm of the internal capsule (**C** and F) shows progressively smaller tract size and misorientation of the pyramidal fibres, directed in both anteroposterior and superoinferior directions compared (C) with the control patient (F).

ities and pontocerebellar hypoplasia. In addition to corpus callosum abnormalities, MRI and tensor diffusion analysis demonstrated that phenotypes resulting from *TUBB3* mutations encompass cortical defects, such as gyral simplification or PMG associated with cerebellar dysgenesis, corticospinal tracts dysgenesis and fibre projection defects. In accordance with the gyral disorganization/simplification and cerebellar dysgenesis presented by all patients, detailed histological investigations showed the presence of unlayered cerebral and cerebellar cortices and heterotopic neurons in the white matter, demonstrating neuronal migration impairment.

Consequently, our findings expand the spectrum of *TUBB3* phenotypes previously described to MCD associated with neuronal migration, organization and/or differentiation defects. However, we cannot exclude the possibility that fine oculomotor nerve defects could be the cause of strabismus in MCD patients described in this study, and the absence of additional ophthalmological impairment indicates that ocular motility disorder, CFEOM3, is not a constant feature of *TUBB3* syndrome as previously described by Tischfield *et al*. (6). Though phenotypes described in this study are different from those reported by Tischfield *et al*. (6), it is worth mentioning this could be the consequence of a bias in patients recruitment due to the distinct ophthalmological and neurodevelopmental research field developed, respectively, by the two laboratories.

Segregation of phenotypes associated with mutations in TUBB3

In contrast with *TUBA1A* and *TUBB2B* mutations, we show that mutations in the *TUBB3* gene are either inherited (three mutations) or *de novo* (four mutations). In all but one of the familial cases, the variations are found in a heterozygous state as they correctly segregate with the phenotype in an autosomal dominant manner and are effected with complete penetrance. The occurrence of familial dominant forms of mild developmental impairment and MCD associated with mutations in the *TUBB3* gene contrasts with the systematic *de novo* occurrence of mutations in *TUBA1A* and *TUBB2B* in association with severe phenotypes.

However, in the case of family 5 which carries the p.A302V mutation, it is worth mentioning that the mother, who is heterozygous for the mutation, is mildly affected, whereas her homozygous daughter is severely affected. These results suggest that *TUBB3* mutations could also exist in a homozygous state and that the severity of the related phenotype is likely to depend on the number of mutated alleles. Nevertheless, the severity of the phenotype presented by a given patient could not only be predicted based on its heterozygous or homozygous status since the *de novo* heterozygous p.T178M and p.M388V mutations are associated with phenotypes which are more severe than the one associated with the homozygote p.A302V mutation.
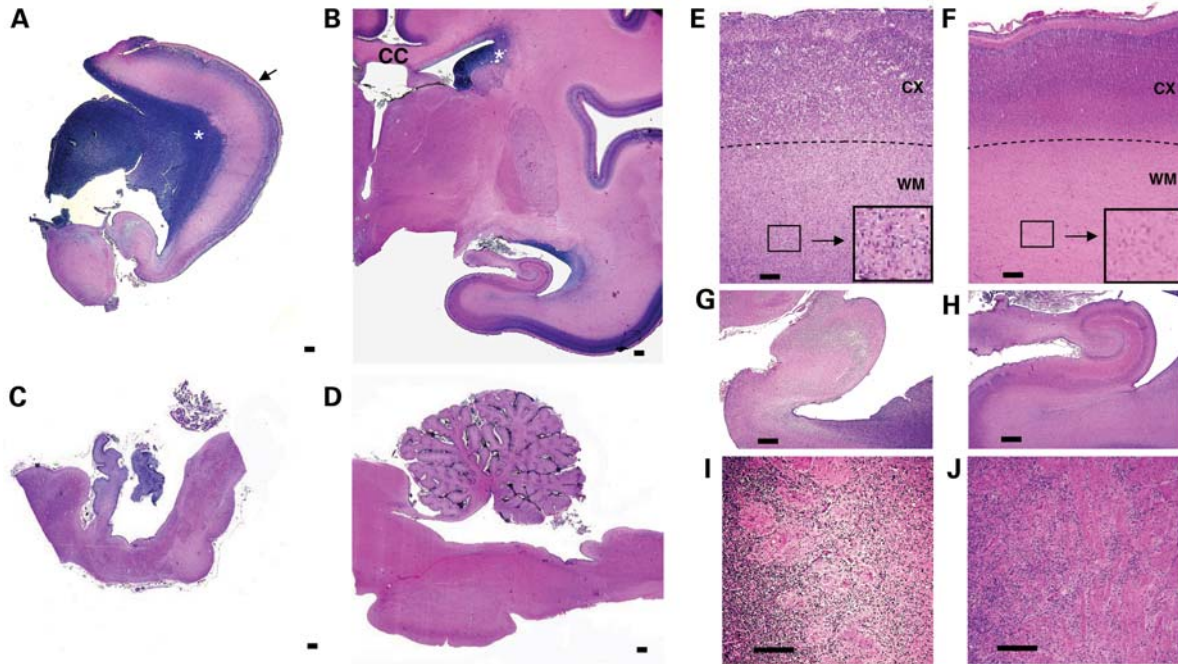
Figure 4. Histopathological analysis of p.M388V fetal case. NissI-stained sections of the 27 GW fetus (**A** and **C**) showing microlissencephaly, corpus callosum agenesis, 'wavy' cortical layer 2 (black arrow), voluminous germinal zone (white asterisk), vermian and cerebellar hypoplasia compared with an age-matched control (**B** and **D**). The histological analysis of the p.M388V fetal case revealed (**E**, **G** and **I**) the presence of gyral abnormalities (festooned-like surface), unlayered cortex with no clear limitation between white and grey matter (E and F), heterotrophic neurons in the white matter (E and F, zoom in black boxes), disorganized hippocampal structures (G and **H**) and abnormal axonal bundles in the ventricular zone (I and **J**). CC, corpus callosum; CX, cortex; WM, white matter. Scale bar: 500 μm (A–D), 100 μm (E–J).

CFEOM3 and MCD mutations alter distinct amino acids

To date, all known variations of the *TUBB3* gene are missense mutations. Neither nonsense mutations nor intragenic deletions have been identified independently from the associated phenotype. In this work, we described six novel *TUBB3* alterations associated with MCD phenotypes, while previously reported mutations (6) are associated with CFEOM3 syndrome, with no cortical abnormalities. Interestingly, the mutations identified in the two studies affect distinct amino acids. However, in the specific case of the A302 amino acid residue, the nature of the variation seems to have a clear influence on the resulting phenotype. Indeed, p.A302T and p.A302V mutations result in CFEOM3 and MCD syndromes, respectively. Although *TUBB3* mutations could lead to a wide range of clinical and imaging phenotypes, it is worth mentioning that recurrent mutations are associated with similar clinical and magnetic imaging features, suggesting that each variation could have a specific consequence on βIII-tubulin function.

Using the model of human β-tubulin developed by Nogales *et al.* (7), we determined the localization of each mutation implicated in MCD or CFEOM3 syndromes within the secondary structure of the βIII-tubulin polypeptide. Detailed analysis shows that three mutated residues in MCD disorders (p.G82, p.T178 and p.M323) were located at the surface of the tubulin, on the opposite side of p.R262, p.E410 and p.D417 mutations reported by Tischfield *et al*. (6), suggesting that these two groups of mutations could impair MTs and/or their interactions with MAPs critical for MT functions in different ways. Our results give evidence that mutations associated with different phenotypes (CFEMO3 versus MCD) might reside in different functional areas of the protein. Thus, in the context of tubulin genes, genotype/phenotype correlations must be assigned not only by considering the primary sequence of the protein, as is classically done, but also by considering the tertiary sequence and the three-dimensional arrangement of the protein. This approach might be more informative as protein interactions largely contribute to MT functions during neuronal migration and differentiation in the context of tubulins and tubulin polymers.

Molecular pathophysiology underlying CFEOM3 and MCD syndromes

One of the intriguing issues raised by *TUBB3* mutations and their associated phenotypes is the allelic phenotypic heterogeneity, i.e. how missense mutations located in the *TUBB3* gene lead either to CFEOM3 or MCD phenotypes. As none of the mutations is common to both studies, it appears at first sight that both the position and the nature of the resulting amino acid from *TUBB3* mutations influence the clinical phenotype. Nevertheless, biochemical experiments show that most of the *TUBB3* variations have the same negative effect on tubulin heterodimerization, independent of the associated phenotype. Indeed, we showed that four of our five tested mutants associated with cortical malformations have an impaired capacity to form αβ heterodimers, probably through GTP-binding-independent mechanisms as none of the mutations localizes in the GTP-binding pocket. These bio-
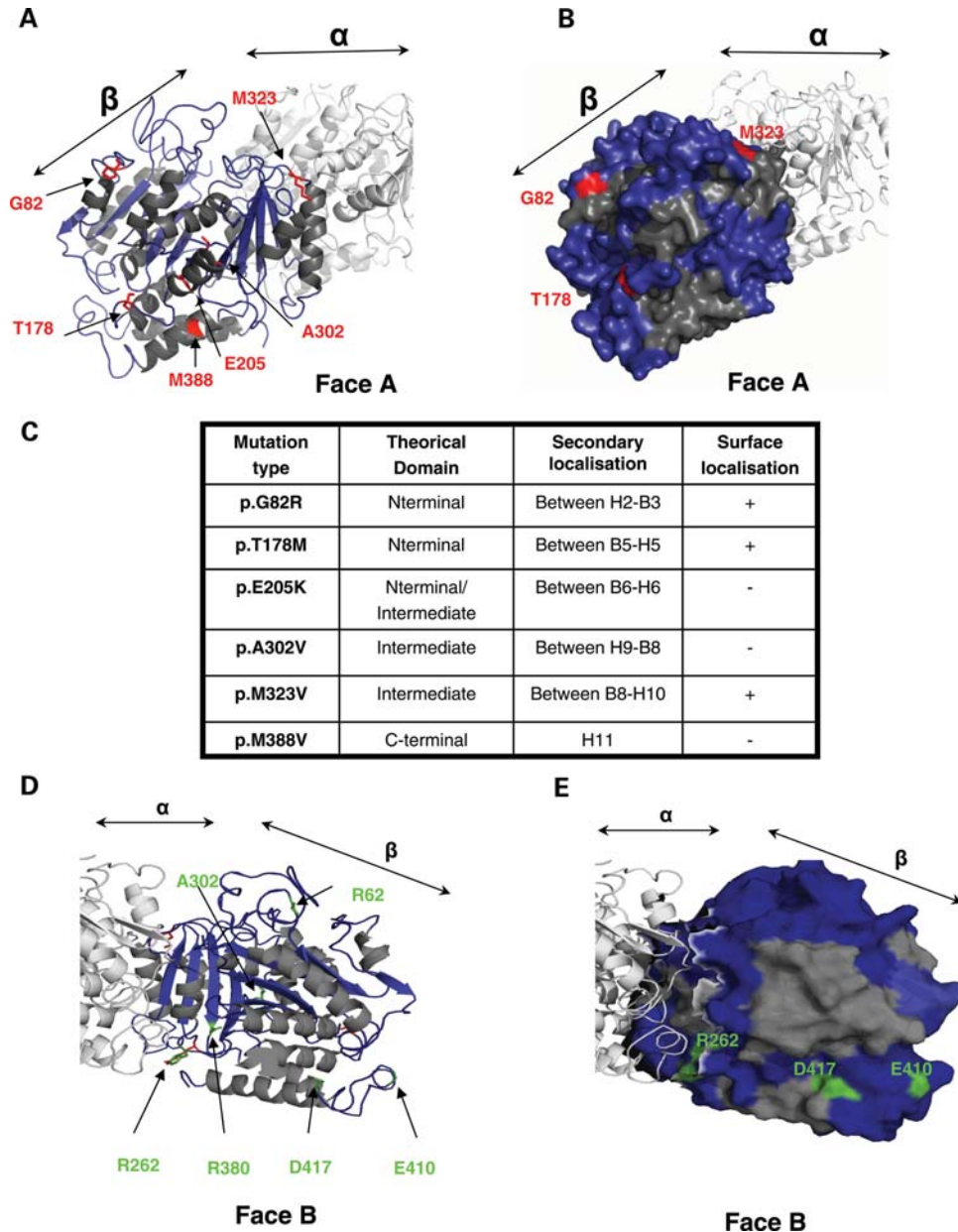
Figure 5. Tubulin structure and positions of *TUBB3* amino acid substitutions associated with MCD, in comparison with *TUBB3* amino acid substitutions associated with CFEOM3. (**A** and **B**) Structural representation (face A) of the α-/β-heterodimer depicted with (A) or without surface delimitation (B), revealing relative positions of MCD *TUBB3* amino acid substitutions either inside the monomer (p.E205K, p.A302V and p.M388V) or on the surface (p.G82R, p.T178M and p.M323V). α- and β-subunits are, respectively, represented in light and dark grey. Contrary to helices that are in grey, β-strands are visualized in dark blue. Localization of *TUBB3* amino acid substitutions is summarized in (**C**). (**D** and **E**) Structural representation (face B) of the α-/β-heterodimer depicted with (D) or without surface delimitation (E), revealing relative positions of CFEOM3 *TUBB3* amino acid substitutions either inside the heterodimer (p.R62, p.A302 and p.R380) or on the surface (p.R262, p.E410 and p.D417). These representations (A–E) show that amino acid substitutions localized on the surface are on opposite sides in case of CFEOM3 (Face B, in D and E) and MCD mutations (Face A, in A and B).

chemical consequences were similar to those described by Tischfield *et al.* who reported the study of eight *TUBB3* mutations implicated in oculomotor disorders. Moreover, cellular analysis demonstrates that in all cases, formed heterodimers are able to fully incorporate into MT networks, suggesting that neither the heterodimerization process nor the incorporation into MTs is a sufficient criterion to explain the phenotype variability observed in *TUBB3* mutations. However, mutation-related specific phenotypes could

potentially result from different consequences on MT dynamics and function, as well as their interacting proteins. This hypothesis is reinforced by the result of cold-treatment experiments suggesting a stability defect of the MT network in fibroblasts bearing p.T178M and p.E205K mutations, as well as by the tri-dimensional modelling discussed above. Interestingly, these findings contrast with those reported by Tischfield *et al.* (6) who pointed out that p.R262C substitution, a mutation shown to be associated with the CFEOM3
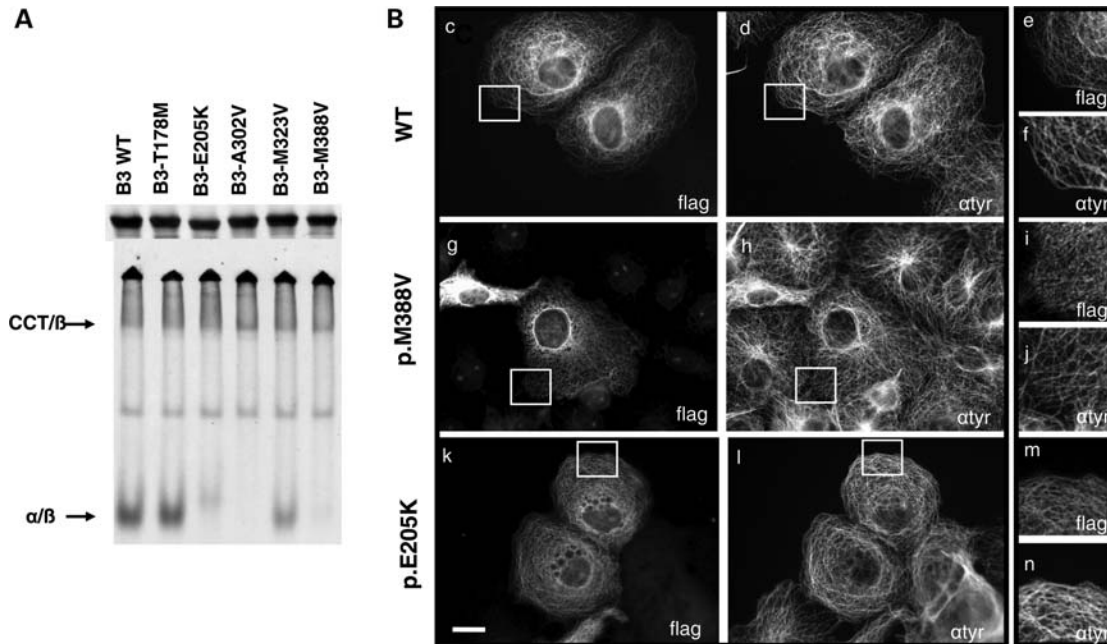
Figure 6. *In vitro* and *in vivo* consequences of *TUBB3* overexpression in WT and mutants concerning heterodimerization processes and MT incorporation. (**A**) Mutations in *TUBB3* result in inefficient α-/β-tubulin heterodimer formation *in vitro*. Analysis by SDS–PAGE and non-denaturing gel of *in vitro* transcription/translation products conducted with ³⁵S-methionine-labelled wild-type (WT) and five different *TUBB3* mutants. The reaction products were further chased with bovine brain tubulin to generate α-/β-heterodimers. SDS–PAGE gel showed that the five mutants were translated as efficiently as the wild type control. Note that in non-denaturing gel condition, p.E205K, p.A302V and p.M388V mutants yielded no discernable amount of α-/β-heterodimers. The p.M323V mutant generated heterodimers comparable to WT control and the remaining mutant p.T178M in a diminished yield. (**B**) Expression of C-terminal FLAG-tagged *TUBB3* wild-type (c–f) and mutants [p.M388V (g–i) and p.E205K (k–n)] in transfected COS7 cells revealed by anti-flag (c, g and k) and anti-tyrosinated α-tubulin (d, h and l) staining. Note the limited dotted pattern of the MT network associated with p.E205K and p.M388V mutants overexpression in some cells (i and m) compared with WT (e) and tyrosinated α-tubulin staining (f, j and n). Scale bar: 20 μm (i).

phenotype, leads to an increased MT stability demonstrated by two different approaches.

Though data reported in this study will contribute to the improvement of the diagnosis of MCDs, deciphering the consequences of *TUBB3* mutation on MT and MAP dynamics and functions, as well as understanding of the phenotypic heterogeneity associated with these mutations, will require further investigations. Together, our findings with the recent data demonstrating the implication of *TUBA8*, *TUBB2B* and *TUBA1A* in cortical dysgenesis disorders should provide further insights to explore the role of MTs in brain development and into how tubulin isotypes dysfunction lead to cortical malformation disorders. Also, in view of the increasing number of tubulin genes shown to be involved in MCD and neurological syndromes, further studies to reveal the full spectrum of disorders associated with mutations in other family members of the tubulin genes will also be of interest.

MATERIALS AND METHODS

Genetic analysis of *TUBB3* clinical assessment

As part of our lissencephaly research programme, we collected samples with diffuse cortical malformations, including the gyral simplification spectrum ($n = 40$), and PMG ($n = 80$) negative for *DCX, LIS1, ARX, TUBA1A, GPR56* and *TUBB2B* mutational screening. We obtained informed consent from parents of affected individuals using protocols

approved by local institutional review boards at L'Hôpital Cochin and INSERM (Medical Research Institute). For each patient, the complete *TUBB3* coding sequence and splice sites were amplified, respectively, in five independent PCR reactions from genomic DNA and were sequenced using the BigDye dideoxy-terminator chemistry and ABI3700 DNA Analyser (Applied Biosystems, Foster city, CA, USA). Primer sequences and PCR conditions are available upon request.

Clinical assessment and imaging analysis

Clinical data were provided by the physicians who are responsible for the medical welfare of the patients. All patients with mutations in *TUBB3* were retrospectively re-examined after the identification of a *TUBB3* mutation. Also, all brain-imaging data were reviewed in order to identify characteristic changes of cortical malformations associated with *TUBB3* mutations. Tractography imaging was realized as previously described in Wahl *et al*. (8).

Neuropathological and immunohistochemical studies

The fetal neuropathological studies were performed after termination of pregnancy at 27 gestational weeks (GW) due to detected malformations, in accordance with French legislation. After removal from the skull, the fetal brain was fixed in a 10% formaldehyde solution containing NaCl (9 g/l) and
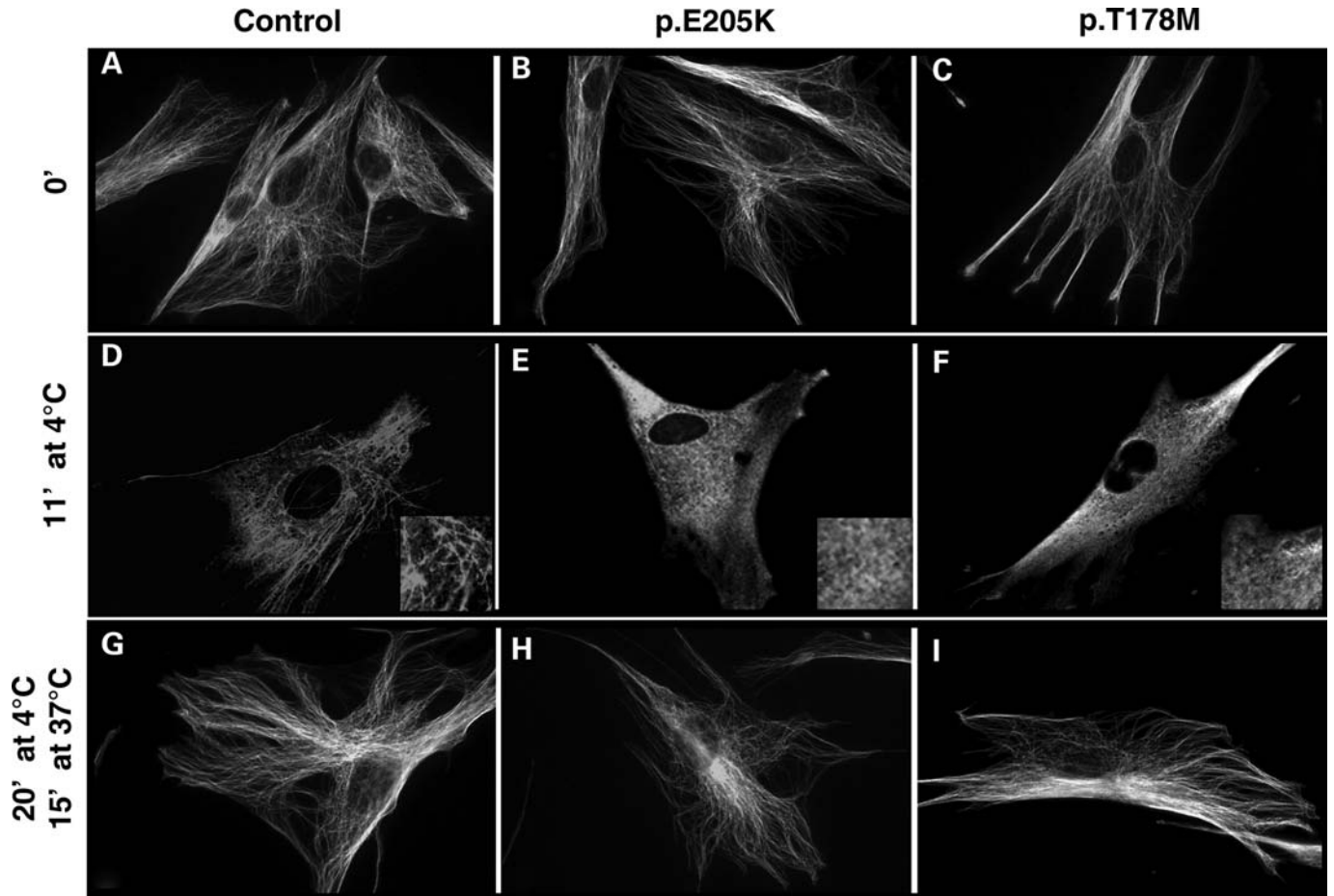
Figure 7. *In vivo* analysis of cytoskeleton behaviour and stability using patients' fibroblasts carrying *TUBB3* p.T178M and p.E205K mutations. Evaluation of the sensitivity of MTs to cold treatment was analysed in control fibroblasts (**A**, **D** and **G**) and patient fibroblasts with p.E205K (**B**, **E** and **H**), p.T178M (**C**, **F** and **I**) *TUBB3* mutations before (A–C) and after 11 min of cold treatment at 4°C (D–E) to show the resistance of MT to depolymerization. Note the increased sensitivity of patient's fibroblasts to cold treatment. The capacity of the cytoskeleton to repolymerize was assessed after 20 min at 4°C and 15 min at 37°C (G–I).

$ZnSO_4$ (3 g/l) for 3–6 weeks according to the volume of the brain. The brain was cut in a coronal plane and sections were embedded in paraffin. Paraffin blocks were cut at either 5 μm (brainstem and cerebellum) or 7–10 μm (hemispheres). Sections were stained with haemalun–phloxin or cresyl violet according to standard methods.

Immunohistochemical procedures were performed at the same time for the mutated patient and one control case of the same age. Paraffin sections were immunostained for glial fibrillary acidic protein with a polyclonal antibody (1:200– 1:400, Dako, USA), vimentin, NeuN (1:500, MAB377, Chemicon), Reelin (1:1000, clone 142) (9), MAP2 (1:100, HM2, Sigma), Calbindin (1:500, Swant Laboratories, Switzerland), Calretinin (1:1000, Swant Laboratories), MIB1 (1:75, Dako) and Tuj1. The Universal Immunostaining System Streptavidin-Peroxydase Kit (Coulter) was used to reveal the reaction. Slides were labelled as previously described in Falletbianco *et al*. (10). After realization, haematoxylin was used to counterstain the brain sections.

All sections were examined under a light microscope (Eclipse 800 Nikon) and some were selected for photographic documentation.

Protein modelling

A model of human β-tubulin was built by homology modelling using available structures (Research Collaboratory for Structural Bioinformatics PDB code 1TUB) from Nogales *et al*. (7). The images in Figure 4 were rendered using PyMOL (http://www.pymol.org).

Cloning and *in vitro* translation

The full-length cDNA encoding the human *TUBB3* sequence was generated by PCR using a template from the human brain cDNA library (Clontech, Mountain View, CA, USA). The PCR product was cloned into the pcDNA 3.1-V5-His vector (Invitrogen, Carlsbad, CA, USA) and checked by DNA sequencing. These products were cloned both into the cDNA3.1-V5-his-TOPO-TA cloning vector (Invitrogen) and pET vector. An in-frame tag encoding the FLAG epitope (DYKDDDDK) was incorporated by PCR along with the C-terminus of the TUBB3 wild-type sequence to allow the distinction of the transgene from other highly homologous endogenously expressed α-tubulin polypeptides. Various

mutations corresponding to those associated with cortical dysgenesis were introduced by site-directed mutagenesis using a QuikChange II kit (Stratagene, La Jolla, CA, USA). All constructs were verified by DNA sequencing. Transcription/translation reactions were performed at 30°C for 90 min in 25 µl of rabbit reticulocyte lysate (TNT; Promega, Madison, WI, USA) containing ^{35}S-methionine (specific activity, 1000 Ci/µmol; 10 µCi/µl). For the generation of labelled α-tubulin heterodimers, transcription/translation reactions were chased for a further 2 h at 30°C by the addition of 0.375 mg/ml of native bovine brain tubulin. Aliquots (2 µl) were withdrawn from the reaction, diluted into 10 µl of gel-loading buffer (gel running buffer supplemented with 10% glycerol and 0.1% bromophenol blue) and stored on ice prior to resolution on a non-denaturing gel (11,12). Labelled reaction products were detected by autoradiography after resolution on either SDS–PAGE or on native polyacrylamide gels as described (11,12).

Cell culture, transfections and immunofluorescence

Primary cultures of fibroblasts were derived from skin biopsies taken from patients with p.T178M and p.E205K mutations and also control patients. HELA and COS7 cells were transfected by variably mutated *TUBB3* constructs using the Fugene 6 transfection reagent (Roche Applied Science, Indianapolis, IN, USA) and grown on glass cover slips in Dulbecco's modified Eagle's medium containing 10% fetal calf serum and antibiotics. The cells were fixed with ice-cold methanol, 24–48 h after growth. In the depolymerization experiments used to determine the stability behaviour of MTs after 24 h of culture, fibroblasts were incubated for various brief intervals from 0 to 30 min on ice and fixed thereafter. Repolymerization experiments were performed by successively exposing cells at 4°C during 20 and 15 min at 37°C. Cells were then labelled with a polyclonal anti-FLAG antibody (1/500), a monoclonal Tuj1 antibody (1/1000) or a monoclonal anti-α-tubulin antibody (1/1000) (DM1A, Sigma-Aldrich Inc., St Louis, MO, USA).

AUTHOR CONTRIBUTIONS

J.C. supervised the design and follow-up of the study and the preparation of the manuscript. K.P. and Y.S. performed genetic and molecular investigations including analysis of mutation consequences on heterodimerization and polymerization, with the help of X.H.J. for biochemical experiments. K.P., Y.S., X.H.J. and J.C. discussed the results. N.L. helped in *TUBB3* screening. N.B.-B. and K.P. recruited cases and controls. N.B.-B., A.R., I.D., C.B., T.A.-B., D.G. and R.N. helped in acquiring patients and parents. N.B.-B. and N.B. re-examined the patients' MRIs and diffusion tensor images. F.E.-R. realized neuropathological analysis and C.F.-B. immunostaining experiments. F.E.-R. and C.F.-B. interpreted neurological analysis of the fetal case. L.C.-P. performed all DNA extractions from subject samples and coordinated interaction with clinicians. B.K. performed Illumina experiments. X.H.J. computed and analysed the structure. K.P. drafted the manuscript with the help of Y.S., N.B.-B., X.H.J. and J.C.

WEB RESOURCES

The URLs for data presented herein are as follows:
Online Mendelian Inheritance in Man (OMIM), http://www.ncbi.nlm.nih.gov/Omim/
University of California-Santa Cruz (UCSC) genome browser, http://genome.ucsc.edu/
NCBI, http://www.ncbi.nlm.nih.gov/
Pymol Molecular Viewer, http://pymol.org

SUPPLEMENTARY MATERIAL

Supplementary Material is available at *HMG* online.

ACKNOWLEDGEMENTS

FUNDING

REFERENCES

1. Keays, D.A., Tian, G., Poirier, K., Huang, G.J., Siebold, C., Cleak, J., Oliver, P.L., Fray, M., Harvey, R.J., Molnár, Z. *et al.* (2007) Mutations in alpha-tubulin cause abnormal neuronal migration in mice and lissencephaly in humans. *Cell*, **128**, 45–57.
2. Poirier, K., Keays, D.A., Francis, F., Saillour, Y., Bahi-Buisson, N., Manouvrier, S., Fallet-Bianco, C., Pasquier, L., Toutain, A., Tuy, F.P. *et al.* (2007) Large spectrum of lissencephaly and pachygyria phenotypes resulting from *de novo* missense mutations in tubulin alpha 1A (TUBA1A). *Hum. Mut.*, **28**, 1055–1064.
3. Jaglin, X.H., Poirier, K., Saillour, Y., Buhler, E., Tian, G., Bahi-Buisson, N., Fallet-Bianco, C., Phan-Dinh-Tuy, F., Kong, X.P., Bomont, P. *et al.* (2009) Mutations in the beta-tubulin gene *TUBB2B* result in asymmetrical polymicrogyria. *Nat. Genet.*, **41**, 746–751.
4. Abdollahi, M.R., Morrison, E., Sirey, T., Molnar, Z., Hayward, B.E., Carr, I.M., Springell, K., Woods, C.G., Ahmed, M., Hattingh, L. *et al.* (2009) Mutation of the variant alpha-tubulin TUBA8 results in polymicrogyria with optic nerve hypoplasia. *Am. J. Hum. Genet.*, **85**, 737–744.
5. Jaglin, X.H. and Chelly, J. (2009) Tubulin-related cortical dysgeneses: microtubule dysfunction underlying neuronal migration defects. *Trends Genet.*, **25**, 555–566.
6. Tischfield, M.A., Baris, H.N., Wu, C., Rudolph, G., Van Maldergem, L., He, W., Chan, W.M., Andrews, C., Demer, J.L., Robertson, R.L. *et al.*

(2010) Human TUBB3 mutations perturb microtubule dynamics, kinesin interactions, and axon guidance. *Cell*, **140**, 74–87.

7. Nogales, E., Wolf, S.G. and Downing, K.H. (1998) Tubulin and FtsZ form a distinct family of GTPases. *Nature*, **391**, 199–202.

8. Wahl, M., Barkovich, A.J. and Mukherjee, P. (2010) Diffusion imaging and tractography of congenital brain malformations. *Pediatr. Radiol.*, **40**, 59–67.

9. de Bergeyck, V., Naerhuyzen, B., Goffinet, A.M. and Lambert de Rouvroit, C. (1998) A panel of monoclonal antibodies against reelin, the extracellular matrix protein defective in reeler mutant mice. *J. Neurosci. Methods*, **82**, 17–24.

10. Fallet-Bianco, C., Loeuillet, L., Poirier, K., Loget, P., Chapon, F., Pasquier, L., Saillour, Y., Beldjord, C., Chelly, J. and Francis, F. (2008) Neuropathological phenotype of a distinct form of lissencephaly associated with mutations in TUBA1A. *Brain*, **131**, 2304–2320.

11. Tian, G., Huang, Y., Rommelaere, H., Vandekerckhove, J., Ampe, C. and Cowan, N.J. (1996) Pathway leading to correctly folded beta-tubulin. *Cell*, **86**, 287–296.

12. Tian, G., Lewis, S.A., Feierbach, B., Stearns, T., Rommelaere, H., Ampe, C. and Cowan, N.J. (1997) Tubulin subunits exist in an activated conformational state generated and maintained by protein cofactors. *J. Cell Biol.*, **138**, 821–832.